Chinese Journal of
POLYMER SCIENCE

RESEARCH ARTICLE

https://doi.org/10.1007/s10118-023-3021-4
Chinese J. Polym. Sci. **2023**, *41*, 1462–1476

Nanoparticle-filled ABC Star Triblock Copolymers: A Dissipative Particle Dynamics Study

Miao Yan[b], Ying-Tong Zhang[b], and Xiang-Hong Wang[a,b*]

[a] *Department of Physics, Shanghai Technical Institute of Electronics & Information, Shanghai 201411, China*
[b] *Department of Physics, Wenzhou University, Wenzhou 325035, China*

Abstract The phase behavior of nanoparticle-filled ABC star triblock copolymers was investigated by dissipative particle dynamics simulation. Two typical structures, the three-color lamella and polygonal tiling structures, were selected to demonstrate the effect of filling the nanoparticle. Results showed that the filling effects were obvious on the lamellar structure but not on the tiling structure, where the high concentration of fillers can destroy the lamellar structures. The dynamic processes of nanoparticle filling were investigated for the lamellar and tiling structures, where three stages can be sorted by analyzing the system energies and chain conformations. Moreover, the mechanical properties were evaluated for the lamellar structures by exploring the interface tensions. The findings can help us understand the potential applications of microstructures based on complex block copolymers and nanoparticle mixtures.

Keywords ABC star triblock copolymer; Dynamic process; Mechanical properties; Nanoparticle

Citation: Yan, M.; Zhang, Y. T.; Wang, X. H. Nanoparticle-filled ABC star triblock copolymers: a dissipative particle dynamics study. *Chinese J. Polym. Sci.* **2023**, *41*, 1462–1476.

INTRODUCTION

The structures self-assembled from block copolymers are gaining increased attention due to their potential applications in emerging areas and the understanding for the basic problems in the self-assembly. Many factors affect the self-assembly of block copolymers, including polymer parameters, topology of polymer chains, confinement environments, polymer gradient, and nanofillers.[1–5] Among these factors, chain topology plays a special role in the self-assembly of block copolymers. For example, ABC triblock copolymers with star topology have distinct features from those of ABC linear triblock copolymers, where the star topology results in several unique self-assembly structures, such as polygonal-tiling structures with translational symmetry.[6]

In ABC star triblock copolymers, the three arms are connected at a conjunction point to form a special topology. The star topology enables the polymer to self-assemble into a series of typical microstructures, ranging from the common layered structures, such as three-color lamella (LAM) structure, to the specialized cylindrical structures with translational symmetry, such as polygonal tile (PT) structure. PT structures have polygonal cross sections and their points of connection are arranged in straight lines, which are extensively observed in experiments.[7–9] These structures have been reproduced in self-consistent field theory (SCFT) calculations and dissipative particle dynamics (DPD) simulations.[10–14] For example, Takano *et al*. reported three types of PT microdomain structures, *i.e.*, (6.6.6), (4.8.8) and (4.6.12), for ABC star triblock copolymers as demonstrated by transmission electron microscopy (TEM). The PT structure was assembled from the prepared ABC star triblock copolymer in bulk, and was observed by TEM after a series of operations, such as annealing, dyeing and slicing. The TEM images showed that the hexagonal cylinders are arranged hexagonally with junction points aligned one dimensionally.[7] Subsequently, these three tiling patterns are confirmed by microbeam small-angle X-ray scattering in addition to TEM.[8] Hayashida *et al*. reported the phase transitions among the PT structures, *i.e.*, [5.3, 5.3, 8], [4.5, 6, 9], [5, 5, 10] and [4, 6.7, 10], by varying the block ratios in the experiments. Usually, triangle phase diagrams are constructed by SCFT calculations based on the block ratios for three blocks in these studies, the closer the position is to the triangle Angle, the higher the volume fraction of one of the three blocks, and the lower the volume fraction of the other two blocks, where the interaction parameters between the blocks are kept constant. For example, Tang *et al*. studied the triangle phase diagram of ABC star triblock copolymers through SCFT calculations and found nine stable microphases, including three-color lamella (LAM) and a series of PT structures.[10] Similar triangle phase diagrams are also constructed using various Flory-Huggins parameters, where the phase behavior of the tiling structures are investigated in detail by SCFT analysis.[11,12] The phase behavior of ABC star tri-

* Corresponding author, E-mail: 20190147@wzu.edu.cn
Special Issue: Theory and Simulation of Macromolecules
Received March 23, 2023; Accepted June 11, 2023; Published online July 19, 2023

block copolymers differs from those in ABC linear triblock copolymers due to the junction constraint at the center of ABC star triblock copolymer and the additional entropy effect. Accordingly, the central knot becomes a powerful topological constraint governing the formation of various geometric structures.

Meanwhile, the nanoparticle (NP) filler provides an alternative method of acquiring desired nanostructures with various properties. Nanocomposites containing NPs and block copolymers have been extensively investigated over the years due to their special properties.[15–30] For example, NPs can enhance the mechanical and optical properties of microstructures compared with those based on neat block copolymers. In turn, the block copolymers can also affect the distribution of NPs in the nanocomposites.[22] In particular, by controlling the dispersion and aggregation of NPs in NP-block copolymer composites, the properties of the composites can be affected.[23–27] Meanwhile, the co-assembly of NPs and block copolymers can break the phase-diagram balance of bulk self-assembly and induce new structures.[28–30] Inevitably, the distributions of NPs and the morphology construction of block copolymers are also important characteristics of nanocomposites.[31–39] For example, Lo *et al*. investigated the effects of thiol-terminated polystyrene-tethered NPs on the morphology of nanocomposite containing poly(styrene-2vinylpyridine) in an experiment. [28] Chen *et al*. used DPD to investigate the effect of NP aggregation on the morphology of block copolymer-NP composites.[26,27] Nanocomposites have a significant impact on nanotechnology with their unique magnetic, optical, electrical, and mechanical properties. Moreover, materials with better 2D and 3D ordered nan oparticles in polymer matrix nanocomposites can also be used as advanced catalysts, selective membranes, and magnetic and photonic band gap materials. However, most of these studies focus on the NP-filled linear block copolymers and the equilibrium states. Therefore, investigating the dynamic processes for the co-assembly of NPs and ABC star triblock copolymers remains necessary.

In the current study, we concentrated on LAM and PT structures for ABC star triblock copolymers to investigate the effects of NP fillers. We used the DPD simulation method to investigate cases of low and high NP concentrations in the dynamic processes. We analyzed the dynamic processes by the molecular conformations and mechanical properties by interfacial tension through the DPD method based on a coarse-grained (CG) model. Section 2 presents the method and model. Section 3 is the results and discussion, and Section 4 shows the summary.

METHOD AND MODEL

Method

We used the DPD method to investigate the ABC star triblock copolymer and NP mixtures in melts. DPD is one of the most efficient mesoscale coarse-grained methodologies for modeling complex fluids, such as soft matter and membrane.[40–45] It was first proposed by Hoogerbrugee and Koelman and improved by Groot and Warren.[46,47] In the DPD method, a group of atoms are coarse grained to be a single bead or particle. These DPD beads interact with one another in a manner according to Newton's law. Three types of forces, namely, conservation force, dissipative force, and random force, are introduced to describe the movement of particles between the i^{th} and j^{th} pairs. These three types of forces are radial along the line between the i^{th} and j^{th} pairs.

Then, the total force acting on the i^{th} particle can be expressed as follows:[40–45,48–50]

$$\mathbf{F}_i = \sum_{j\neq i}(\mathbf{F}_{ij}^{C} + \mathbf{F}_{ij}^{D} + \mathbf{F}_{ij}^{R}) \tag{1}$$

where the sum runs over all other particles within a certain cutoff radius r_c. The conservative force $\mathbf{F}_{ij}^{C}$ is a soft repulsion force that describes the interaction among coarse-grained particles, which can be expressed as follows:

$$\mathbf{F}_{ij}^{C} = a_{ij}\left(1 - \frac{r_{ij}}{r_c}\right)\hat{\mathbf{r}}_{ij} \tag{2}$$

where the subscript index ij refers to the relative quantity between the i^{th} and j^{th} particles; and a_{ij} is the repulsion parameter between the i^{th} and j^{th} particles, which is related to the Flory-Huggins χ-parameter.[47] Here, $\mathbf{r}_{ij} = \mathbf{r}_i - \mathbf{r}_j$ is the relative position between the i^{th} and j^{th} particles, and $\hat{\mathbf{r}}_{ij} = \mathbf{r}_{ij}/|\mathbf{r}_{ij}|$ is the unit vector where the norm $r_{ij} = |\mathbf{r}_{ij}|$. The conservative force vanishes beyond the cutoff distance r_c. Dissipative force $\mathbf{F}_{ij}^{D}$ represents the viscous resistance among moving particles, and it has a linear relationship with the velocity:

$$\mathbf{F}_{ij}^{D} = \gamma\left(1 - \frac{r_{ij}}{r_c}\right)^2(\hat{\mathbf{r}}_{ij}\cdot\mathbf{v}_{ij})\hat{\mathbf{r}}_{ij} \tag{3}$$

where $\mathbf{v}_{ij} = \mathbf{v}_i - \mathbf{v}_j$ represent the relative velocity, and γ is the friction coefficient. The random force $\mathbf{F}_{ij}^{R}$ is a stochastic force, which can be expressed as follows:

$$\mathbf{F}_{ij}^{R} = \sigma\left(1 - \frac{r_{ij}}{r_c}\right)^2\zeta_{ij}\Delta t^{-1/2}\hat{\mathbf{r}}_{ij} \tag{4}$$

where ζ_{ij} represents a randomly distributed value between 0 and 1 with a Gaussian distribution; σ is the noise amplitude. γ and σ are related as $\sigma^2 = 2\gamma k_B T$, where T is the absolute temperature, and k_B is the Boltzmann constant; $\sigma = 3.0$ and $\gamma = 4.5$ are usually used as standard values in the simulation.[51]

Then, the motion of the i^{th} particle is governed by Newton equations of motion,

$$m_i\frac{d\mathbf{v}_i}{dt} = \mathbf{F}_i, \frac{d\mathbf{r}_i}{dt} = \mathbf{v}_i \tag{5}$$

where m_i is the mass of the i^{th} particle. To solve these equations, the velocity-Verlet algorithm was used in the simulation, which has been proven to be efficient:[40,52]

$$\begin{aligned}
&\mathbf{r}_i(t+\Delta t) = \mathbf{r}_i(t) + \Delta t\mathbf{v}_i(t) + 1/2(\Delta t)^2\mathbf{f}_i(t)\\
&\tilde{\mathbf{v}}_i(t+\Delta t) = \mathbf{v}_i(t) + \lambda\Delta t\mathbf{f}_i(t)\\
&\mathbf{f}_i(t+\Delta t) = \mathbf{f}_i(\mathbf{r}(t+\Delta t), \tilde{\mathbf{v}}_i(t+\Delta t))\\
&\mathbf{v}_i(t+\Delta t) = \mathbf{v}_i(t) + 1/2\Delta t(\mathbf{f}_i(t) + \mathbf{f}_i(t+\Delta t))
\end{aligned} \tag{6}$$

where, Δt is time step in the simulations. The entire simulation was performed under the NVT ensemble system by using large-scale atomic/molecular massively parallel simulator.[53]

Model

Star triblock copolymers have been modeled in MC simulations and SCFT simulations, in which CG models are extensively used.[11,12,54–57] However, we choose to use DPD method

because compared with MC simulation and SCFT simulation, DPD simulation can better study the dynamic process and mechanical properties in the simulation. In the current DPD simulation, we used a simple CG model, in which a group of molecules were coarse grained into a particle, as shown in Fig. 1. In the star topology, three arms were connected at a point, and these chains repulsed one another. The atomic representation of the ABC star triblock copolymer is shown in Fig. 1(a). The atomic clusters circled by the dotted lines are coarse-grained DPD beads. Red, blue, and yellow represent chains A, B, and C, respectively, is also shown in Fig. 1(b). NPs are the purple particles as shown in Fig. 1(c). An example of the NP-filled microstructures is also shown in Fig. 1(d). These consecutive particles connected with an additional elastic harmonic force:

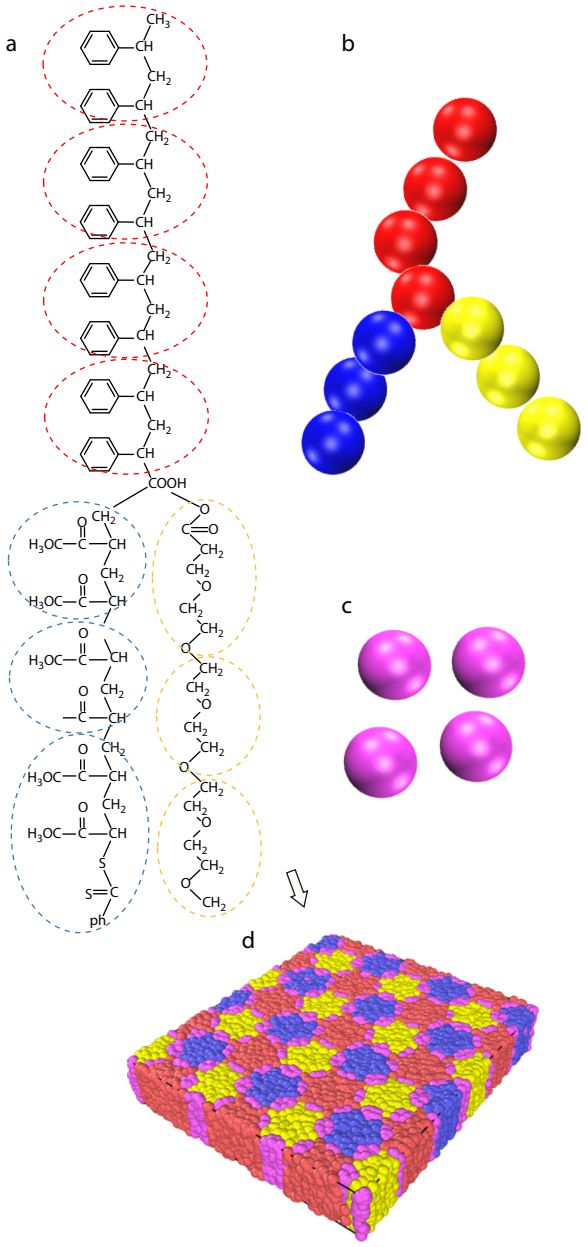

Fig. 1 Self-assembly of ABC star triblock copolymers and NPs. (a) The atomistic representation of ABC star triblock copolymer is demonstrated in the left and (b, c) the coarse-grained of ABC star triblock copolymer and NPs models are in the right, (d) the microstructure with a volume fraction of is in the below. The red, blue and yellow colors represent A-, B- and C-blocks, respectively, and NPs are represented in purple colors.

$$\mathbf{F}_{ij} = k_s(1 - \frac{r_{ij}}{r_s})\hat{\mathbf{r}}_{ij} \tag{7}$$

where k_s and r_s are the spring constant and equilibrium bond length, respectively. Based on previous works,[51,58] we adopted k_s = 120.0 and $r_s = 0.7r_c$ in the current simulation. To adjust chain flexibility, an extra bending force caused by a harmonic constraint on two consecutive was introduced:[33,59–61]

$$\mathbf{F}^{\theta} = -\nabla[\kappa(\theta - \theta_0)] \tag{8}$$

where, κ, θ_0 = 180° and θ are the bending constant, equilibrium angle and inclination angle, respectively.

As for the model of NPs, there are many modeling methods according to the specific situation. For example, atomic modelling—NPs are made of single atoms and are small in size; Low coarse-grained modeling—NPs are composed of multiple beads to form a single bead with a larger size; High coarse-grained modeling—NPs consist of multiple atomic clusters, are relatively small in size.[62] In most cases, the size of the NP model chosen is relatively large and rigid, which can be better distinguished from other molecules in the system,[18,36,37,51,62–64] such as endocytosis of the membrane,[62] penetration of the NP in the membrane,[51,62] and graft of the NP onto the polymer.[18,36,37] In other cases, NPs are modeled to be small in size and not rigid (*e.g.*, NPs made of colloids or polymers).[24,65] The model we chose for the NPs is rather crude, coarse-grained into a simple DPD particle composed of atomic clusters. We focus on the effect of NPs on the assembly of the polymer when the number of NPs is similar to that of one of the polymer blocks, ignoring the effects of the NP size and shape. In the current simulations, we modeled the NP as a simple one DPD particle, similar to those in previous works.[26,27,33,62,66] There have also been other studies in which the NPs have been modelled as a simple DPD beads, but with different sizes.[63,67–69] There are, of course, more complex models of NPs.[70,71,72]

Parameters

The parameters can be classified as polymer and simulation parameters. The parameters in star triblock copolymers are complex, so they cannot be used to explore the properties of star triblock copolymers in full-parameter space. Hence, we investigated the ABC star triblock copolymers in a subspace by fixing several polymer parameters. In the current simulation, we set the repulsive interaction parameters between two DPD particles, namely, a_{ii} = 15 and a_{ij} = 45, for the same and different types of particles in the simulations, which is applied extensively in previous works.[40,73] For a description in detail, the interaction parameters are shown in Table 1, in which the other parameters are also listed. Thus, there is a repulsive interaction between NPs, which can avoid overlapping and infiltration between NPs as much as possible. The interaction parameters in DPD related to the Flory-Huggins parameter proposed by Groot and Warren was adopted:[47]

$$\chi = 0.689\,(a_{ij} - a_{ii}) \tag{9}$$

https://doi.org/10.1007/s10118-023-3021-4

Table 1 System parameters in the simulation box.

DPD parameters	p=5	σ=3.0		γ=4.5
a_{ij} Beads / Beads				
	15			
	45	15		
	45	45	15	
	45	45	45	15

 are the A-, B- and C-blocks of ABC star triblock copolymer, respectively,  is NP.

where $\rho = 5$ is the particle density. Hence, the Flory coefficient between two different beads is about 20.67, which is located in the strong segregated regime. The chain length plays an important role in the properties of star triblock copolymers. In the current simulations, we set the chain length to be two cases, *i.e.*, $f_A:f_B:f_C = 0.5:0.4:0.1$ and $f_A:f_B:f_C = 0.4:0.3:0.3$; and we set the radius of NP to be $r = r_c$. In these two cases, we adjusted the polymer-flexibility parameter κ and the concentration of NPs Φ_{NP}.

In the DPD simulations, the mass, length, and time were scaled to be unity. In particular, the mass of DPD particle m was taken as 1, and the length was scaled to be the cutoff radius r_c. The cutoff radius was related to $r_c = (\rho V_p)^{1/3}$, where V_p denotes the volume of individual particle.[47] The time was scaled as the normalized unit τ, defined as follows:

$$\tau = r_c\sqrt{m/k_BT} \tag{10}$$

where, m is the particle mass, k_B is the Boltzmann constant, and T is the temperature. k_BT is the energy scale. In the current simulations, we set the timestep $t = 0.05\tau$ in the modified velocity-Verlet algorithm.

We performed our DPD simulations similar to the previous works.[74,75] In particular, we set the periodic boundary conditions of three directions in the current simulations, and the simulation is limited to a cubic box with three side lengths of $L_x \times L_y \times L_z$. To avoid the effect of finite size,[76] we optimized the box size by trial and error and used various box sizes with $L = 10 - 30r_c$ in different polymer systems. We set the total DPD time steps as 200000 in the dynamic process to obtain equilibrium structures. The system can reach the equilibrium state when the process was about 200000 DPD time steps, and an example is shown in Fig. 2. Moreover, the system pressure and temperature were uniformly distributed throughout the simulation boxes. We used multiple initial states to acquire a structure with the minimum energy value. Then, we selected the structure with the lowest energy as the most stable structure in the simulations.

RESULTS AND DISCUSSION

We selected two typical structures by fixing the block ratios, *i.e.*, LAM with $f_A:f_B:f_C = 0.5:0.4:0.1$ and the PT with $f_A:f_B:f_C = 0.4:0.3:0.3$. We adjusted two parameters, the NP concentration Φ_{NP} and the polymer flexibility parameter κ, to investigate the dynamic processes and mechanical properties of ABC star triblock copolymers. The microstructures of NP-filled ABC star triblock copolymers are presented in subsection IIIA (Figs. 3 and 4); We concentrated on the dynamic processes for the LAM structures with various NP concentrations in subsection IIIC (Figs. 5–9), and mechanical properties for LAM structures with various Φ_{NP} and κ values in subsection IIID (Figs. 10 and 11).

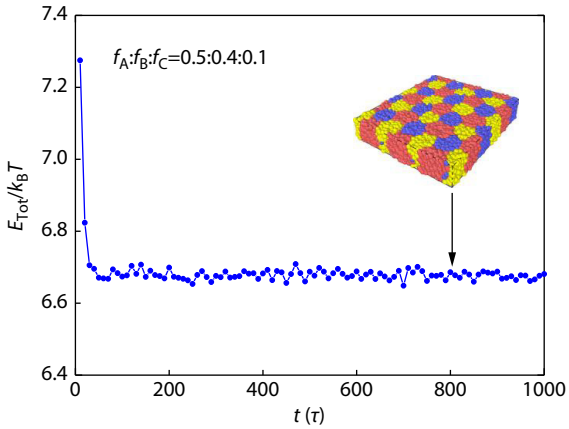

Fig. 2 An example for obtaining the equilibrium state in the dynamic process. The total energy E_{Tot}/k_BT as function of time steps. The inset represents the morphology of ABC star triblock copolymers at the time step of 800τ.

Microstructures of NP-filled ABC Star Triblock Copolymers

We considered typical bulk structures for ABC star triblock copolymers, which have been investigated in experiments and self-consistent field theory calculations. Two typical bulk structures, LAM and PT structures, were taken as examples. We demonstrated the lamellar structures with $f_A:f_B:f_C = 0.5:0.4:0.1$ in Fig. 3. The bulk structures without NPs are shown in Figs. 3(a1) and 3(a2), where the lamellar structures are illustrated. Fig. 3(a1) shows the density distributions in two-dimensional space, *i.e.*, the *x*-*z* plane, indicating that the A-, B- and C-blocks self-assembled into the triple lamellar structures. To clearly demonstrate the lamellar structures, we plotted the volume fractions as functions of positions along the *z* axis for the A-, B- and C-blocks, respectively, as shown in Fig. 3(a2). The C-blocks were distributed between the A- and B-block domains. Our DPD simulations about the lamellar structures agreed with previous SCFT calculations and experimental observations, where lamellar with three alternative colors have been observed.[7,10,12,13] Then, we added a small number of NPs, *i.e.*, $\Phi_{NP} = 0.005$, into the LAM structure, as shown in Figs. 3(b1) and 3(b2), where the triblock copolymers and NPs are demonstrated. Fig. 3(b1) indicates that the ABC star triblock copolymers maintained their lamellar structure when small numbers of NPs were added, which was probably due to the strong repulsive interactions among different blocks.[77] We further observed that the NPs were distributed between the distinct block domains in the ABC star triblock copolymer matrix. This finding was similar to those observed in the diblock copolymer matrix in the experimental and SCFT calculations, where the NPs were distributed between the A- and B-block

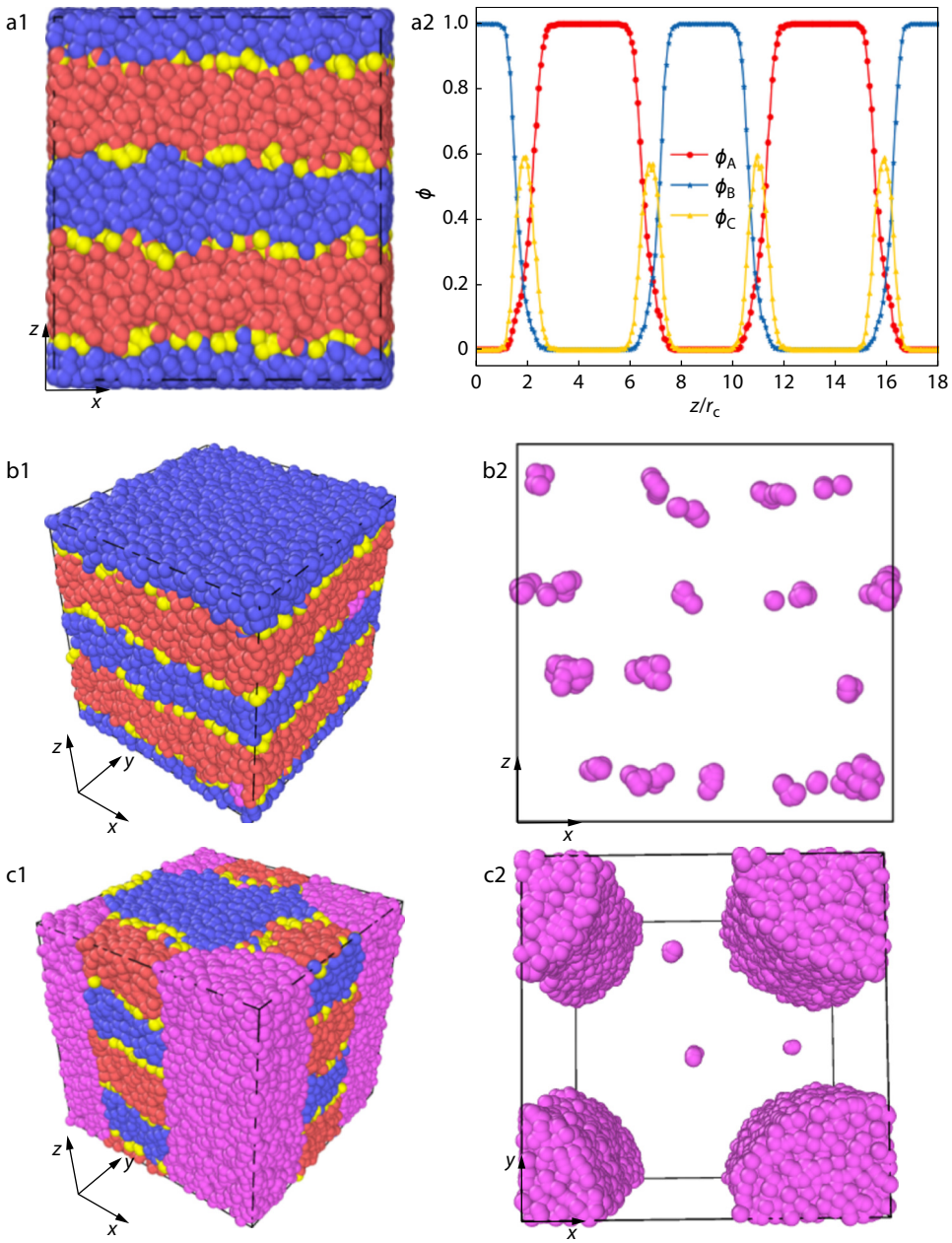

Fig. 3 The LAM and NP composites. The volume fractions of LAM are $f_A:f_B:f_C=0.5:0.4:0.1$. (a) The morphology of LAM with the NP concentration of Φ_{NP} = 0. The top view is in the left (a1) and the density profiles of A-block, B-block and C-block chains is in the right (a2). (b) The NP concentration is Φ_{NP} = 0.005. The morphology of LAM is in the left (b1) and NP distribution is in right (b2). (c) The NP concentration is Φ_{NP} = 0.330. The morphology of LAM is in the left (c1) and NP distribution is in right (c2). The red, blue and yellow colors represent A-, B- and C-blocks, respectively, and NPs are represented in purple colors.

domains.[23,78–80] This fact suggested that entropy played an important role in the NP-directed distributions. When the numbers of NPs were increased to be high concentration of $\Phi_{NP}=0.330$, we observed a special structure, as shown in Figs. 3(c1) and 3(c2). In this structure, the ABC star triblock assembled into an unperfected lamella but with flat interfaces, whereas the NPs were pushed into four columnar zones. The previous DPD simulation suggested that the large numbers of NPs led to the twisting of lamellar structures in the diblock copolymer matrix, in which the NP concentration exceeded 0.2.[81] Herein, we observed that the LAM with the star topologies limited the distortion of flat interfaces instead of enforcing the NPs into cylinder domains. This phenomenon provided a possible way to acquire the NP aggregation shape by directed assembly with star triblock copolymers. The polymer-based nanocomposites can be used as catalysts, magnetic materials, photoengraving, food packaging and more.

Additionally, we demonstrated the NP-filled structures of star triblock copolymers with $f_A:f_B:f_C$ = 0.4:0.3:0.3, as shown in Fig. 4. In the bulk structure without NPs, the ABC star triblock copolymers had a tiling structure, as shown in Figs. 4(a1) and 4(a2). This PT structure belonged to the [6.6.6] tiling pat-

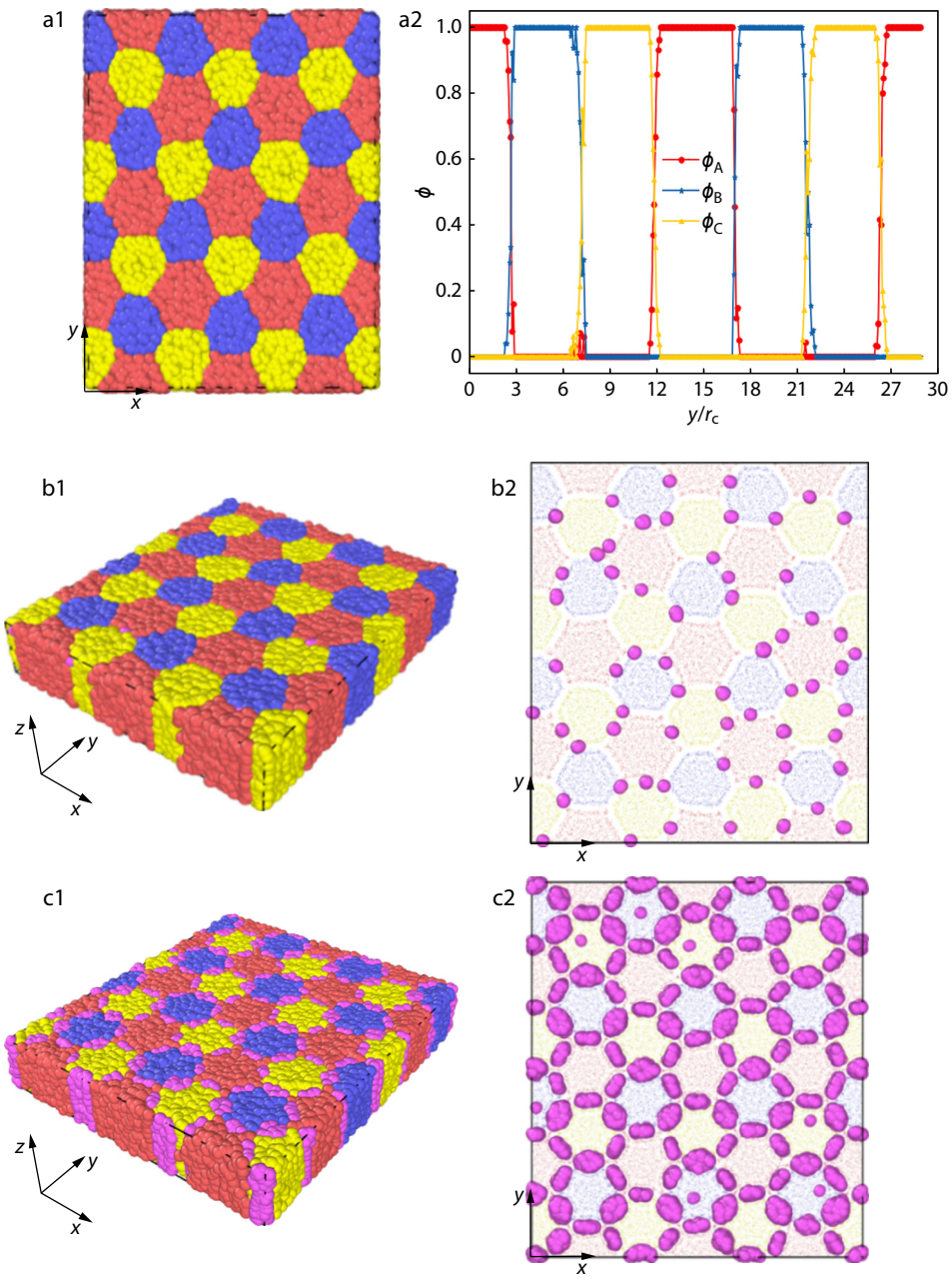

Fig. 4 The PT and NP composites. The volume fractions of PT are $f_A:f_B:f_C=0.4:0.3:0.3$. (a) The morphology of PT with the NP concentration of Φ_{NP} = 0. The top view is in (a1) and the density profiles of A-block, B-block and C-block chains are in (a2). (b) The NP concentration is Φ_{NP} = 0.003. The morphology of PT is in (b1) and NP distribution is in (b2). (c) The NP concentration is Φ_{NP} = 0.232. The morphology of PT is in (c1) and NP distribution is in (c2). The red, blue and yellow colors represent A-, B- and C-blocks, respectively, and NPs are represented in purple colors.

tern,[11] as shown in Fig. 4(a1), and the sharp density profiles in Fig. 4(a2) indicated that the phase separation was located in the strong segregation region. Our observation about the PT structure with $f_A:f_B:f_C$ = 0.4:0.3:0.3 was the same as the previous experimental and SCFT results, although the interactions between blocks were stronger than those in previous works.[7–12,14] To examine the effects of filling NPs, we added NPs with various concentrations into the PT structures, as shown in Figs. 4(b) and 4(c), respectively. For the low concentration with Φ_{NP} = 0.003, we observed that the triblock copolymer matrix retained the PT pattern, as shown in Fig. 4(b1). The NPs were distributed among the various cylinder domains, as shown in Fig. 4(b2), similar to previous studies, where NPs are uniformly distributed at the interfaces among block domains.[26,27] Various distributions of NPs were found in the diblock copolymer matrix where the NPs were located within the cylinder block domains due to the shape of particles.[82] For the high concentration with Φ_{NP} = 0.232, we observed that the triblock copolymer matrix retained the PT pattern, as shown in Fig. 4(c1). We observed as well that the NPs were not scattered and instead uniformly distributed at the interfaces between the various hexagonal domains, as

https://doi.org/10.1007/s10118-023-3021-4

shown in Fig. 4(c2). This is due to the repulsive interactions between the different beads of DPD that tend to separate, while the star topology, the presence of the copolymer central junction, gives the copolymer connectivity and prevents its macroscopic separation. In addition, the ratio of the volume fraction of each block in the PT structure is 0.4:0.3:0.3, which makes the volume fraction of each block similar. In this way, when the system reaches equilibrium, the position of the central node is not easily disturbed. Therefore, PT structure is more stable than LAM structure. Notably, the distributions of NPs had the same translation asymmetry as the star triblock copolymer matrix. This translation along the *z* axis originated from the special star topology of the triblock copolymer matrix, which enforced the joint points of star blocks arranged into a line.[7] It can be observed that the star topology has a strong constraint on the PT structure, resulting in a small effect of nanoparticles on the PT structure. Here, our observation provided a possible way for the aggregation of NPs with desired patterns.

Dynamic Processes of NP-filled ABC Star Triblock Copolymers

In this subsection, we investigated the formation processes for the structures of NP-filled ABC star copolymers by analyzing the system free energy, mean square radius of gyration, and shape factor. We concentrated on the LAM structure and PT structure, and took the low- and high- concentrations of NPs, as two examples to evaluate the dynamic processes.

We plotted the energies as functions of step time, as shown in Fig. 5, where the typical structures were also inserted. In both cases, the evolution processes can be divided into three stages: initial, adjustment, and stable. For low-concentration NP with $\Phi_{NP}=0.005$, as shown in Fig. 5(a), we analyzed the energy evolution in the dynamic processes and the spatial distribution of NPs. When $t=0\tau$ and $E_{Tot}/k_BT=5.69$, the NPs were distributed randomly in space. In the initial stage of $0-100\tau$, the free energy rapidly decreased and NPs tended to be distributed in an orderly manner. When $t=100-300\tau$, the energy slightly oscillated and showed a weak downward trend, in which the NPs and lamellar structure were in the adjustment stage. When $t=300-1000\tau$, the process was in the stable stage for a long time, and the energy of the system reached the corresponding stable value, $E_{Tot}/k_BT=5.45$. In this stage, the structure reached the equilibrium state. For the high concentration with $\Phi_{NP}=0.330$, as shown in Fig. 5(b), the dynamic process differed from that shown in Fig. 5(a). Specifically, when $t=0\tau$, the energy $E_{Tot}/k_BT=7.50$ was much higher than those in the $\Phi_{NP}=0.005$ case, although the initial input was randomly distributed similar to the $\Phi_{NP}=0.005$ case. At the initial stage of $t=0-230\tau$, the structure obviously changed and the energy rapidly decreased. Afterwards, the structure turned to the adjustment stage with $t=230-830\tau$. In this stage, the structure continued to adjust, and energy had a slow downward trend. During this period, NPs gradually clustered into columns at the four corners of the space. When $t=830-1000\tau$, the system developed into the stable stage, and the energy and structure tended to be stable. In this stage, NPs gathered in columnar shape on the four angles of $x=0-4.0r_c$ and $x=12.0-20.0r_c$ along the *z*-axis. Here, we compared the dynamic-evolution processes under the influence of low and high concentration NPs. For high-concentration NPs, the initial and adjustment stages were longer, and the time to reach equilibrium was also longer. Previous studies have reported the dynamic paths of NP aggregation in the melt of diblock copolymers and NPs.[26,27] This process is demonstrated by analyzing the morphology and nanoparticle distribution at different times. Here, we observed that the dynamic processes of the system were similar to those observed in other cooperative self-assembly systems of block copolymers and NPs.[24,26,27] But we analyzed the process in three stages by combining the free energy of the system with the distribution of the nanoparticles.

Meanwhile, we plot the dynamic process of self-assembly of the PT structure with NPs at different concentrations. The evolution process is still divided into three stages: initial stage, adjustment stage and stable stage, in which the typical spatial distribution maps of NPs at different stages in the simulation process are inserted, as shown in Fig. 6. Fig. 6(a) shows the situation where a small number of NPs are added, *i.e.*, the

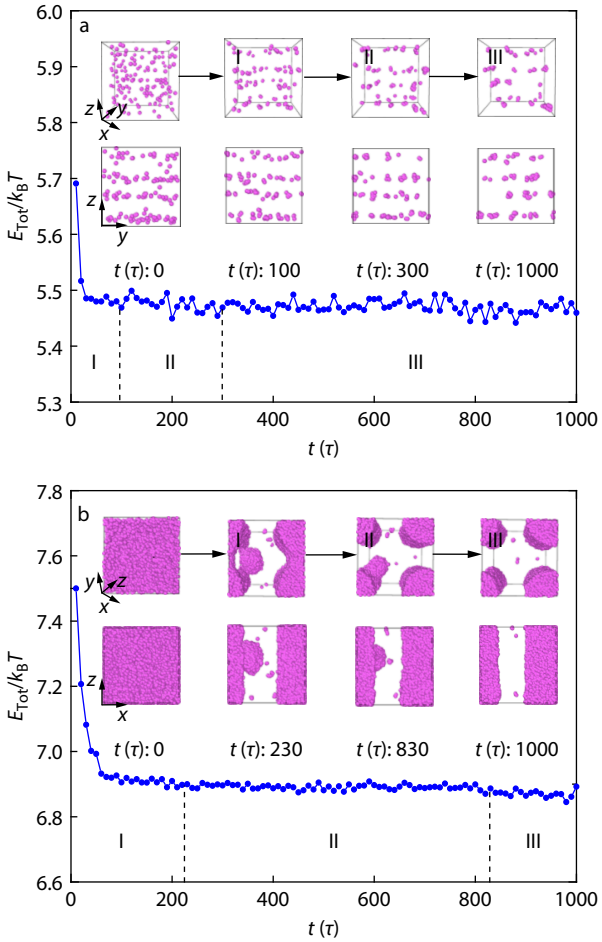

Fig. 5 The dynamics processes for LAM with the volume fractions of f_A:f_B:f_C=0.5:0.4:0.1 The total energy E_{Tot}/k_BT as function of the time steps are shown. (a) The insets represent the distribution of NPs at the time steps of 0τ, 100τ, 300τ, and 1000τ, respectively, at the low NP concentration of $\Phi_{NP}=0.005$. (b) The insets represent the distributions of NPs at the time steps of 0τ, 230τ, 830τ, and 1000τ, respectively, at the high NP concentration of $\Phi_{NP}=0.330$. The NPs are represented in purple colors.

https://doi.org/10.1007/s10118-023-3021-4

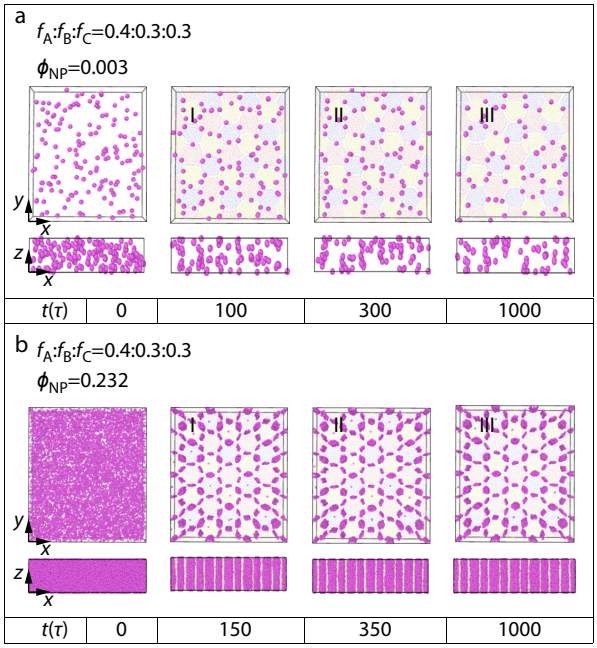

Fig. 6 The dynamics processes for PT with the volume fractions of f_A:f_B:f_C=0.4:0.3:0.3. (a) The insets represent the distribution of NPs at the time steps of 0τ, 100τ, 300τ, and 1000τ, respectively, at the low NP concentration of Φ_{NP} = 0.003. (b) The insets represent the distributions of NPs at the time steps of 0τ, 150τ, 350τ, and 1000τ, respectively, at the high NP concentration of Φ_{NP} = 0.232. The NPs are represented in purple colors.

volume fraction is Φ_{NP} = 0.003. When t = 0τ, the NPs are randomly distributed. In the initial stage, during t = 0−100τ, the ABC star triblock copolymer self-assembles to form a PT structure, while the NPs move rapidly to the junction of hexagonal columns formed by different blocks, and begin to show an orderly distribution trend in the whole space. When t = 100−300τ, the structure of PT and NPs is in the adjustment stage, the distribution of NPs is no longer too dispersed and begins to gather. When t = 300−1000τ, the process is in a stable stage for a long time, the system reaches an equilibrium state, and the evolution of PT structure and NPs no longer occurs. The NPs are aggregated and distributed in different blocks forming hexagonal column junctions. The situation of NPs with filled volume fraction is Φ_{NP} = 0.232, shown in Fig. 6(b). The initial input is also randomly distributed, similar to the addition of low-concentration NPs. When t = 0−150τ, the system is in the initial stage, the structure has changed obviously. While the ABC star triblock copolymer self-assembled to form the PT structure, most of the NPs moved rapidly towards the junction of hexagonal columns formed by different blocks, and a few remained in the region of hexagonal columns formed by different blocks. Then, when t = 150−350τ, in the adjustment phase, a small number of NPs in the region of hexagonal columns formed by different blocks gradually move towards the junction of hexagonal columns formed by different blocks. When t = 330−1000τ, the system develops to a stable stage and the structure is in a state of equilibrium. At this stage, the NPs aggregate towards the junction of hexagonal columns formed by different blocks, and the junctions of each block of the PT structure assembled by the ABC star triblock copolymer body are arranged in a line. By comparing the dynamic evolution process under the influence of low and high-concentration NPs, we can see that in the case of doping high-concentration NPs, the initial stage and adjustment stage are longer, and the time to reach equilibrium is longer. However, compared with the dynamic process of self-assembly of LAM structures and NPs, the initial and adjustment stages become very short. This also indicates that the PT structure is more stable than the LAM structure.

Then, we considered the mean-square radius of gyration in the dynamic processes. Actually, the mean square radius of gyration $\mathbf{R}_g^2$ is a tensor that can be expressed as follows:[83,84]

$$\mathbf{R}_g^2 = \begin{pmatrix} R_{gxx}^2 & R_{gxy}^2 & R_{gxz}^2 \\ R_{gyx}^2 & R_{gyy}^2 & R_{gyz}^2 \\ R_{gzx}^2 & R_{gzy}^2 & R_{gzz}^2 \end{pmatrix} \tag{11}$$

where the element $R_{g\alpha\beta}^2$ is

$$\left\langle R_{g\alpha\beta}^2 \right\rangle = \frac{1}{N}\sum_i \left\langle \left(r_{i,\alpha} - r_{c,\alpha}\right)\left(r_{i,\beta} - r_{c,\beta}\right) \right\rangle \tag{12}$$

with $\alpha, \beta \in \{x, y, z\}$, where $r_{i,\alpha}$ and $r_{c,\alpha}$ represent the α-coordinate of the i^{th} particle and the center of mass, respectively; and N is the number of chains.

We demonstrated the dynamic processes by the mean-square radius of gyration in Fig. 7. For the low volume fraction of NPs with , as shown in Fig. 7(a), we plotted the three components R_{gxx} , R_{gyy}, R_{gzz} of R_g in the dynamic processes, according to Eqs. (11) and (12). Results showed that the average values of and were relatively close and greater than those of when the number of NPs was small, indicating that the LAM structures were relatively stretched in the x-direction and y-direction but compacted along the z-direction. Actually, the addition of low-concentration NPs was similar to those without NPs, where the average values of and were also relatively close and greater than those of R_{gzz}. This result was similar to the formation process previously observed in phospholipid membranes.[75,85] For high-concentration , as shown in Fig. 7(b), this was not the case. The average values of R_{gyy} and R_{gzz} were relatively close and greater than those of R_{gxx}, indicating that the lamella structures were relatively stretched in the y-direction and z-direction but compacted in the x-direction. This finding was due to the effect of NP cylinders that pushed the triblock copolymers along the z-direction. Moreover, for low-concentration NPs, the mean-square radius of gyration did not significantly change, indicating that the lamellar structure did not change in three stages. However, in the case of adding high-concentration NPs, the mean-square radius of gyration changed and the values of the three components of exceeded the previous two cases, indicating that the structural changes were relatively larger. This finding was consistent with our simulation observations that the structures exhibit three stages in the dynamic processes.

Meanwhile, we also plotted the gyration radius of the PT structure, as shown in Fig. 8. The dynamic process is different from that of LAM structure. For the filled low-concentration NPs with volume fraction of Φ_{NP} = 0.003, as shown in Fig. 8(a), we observed three components in the dynamic process R_{gxx}, R_{gyy}, R_{gzz}. The results show that when the concentration

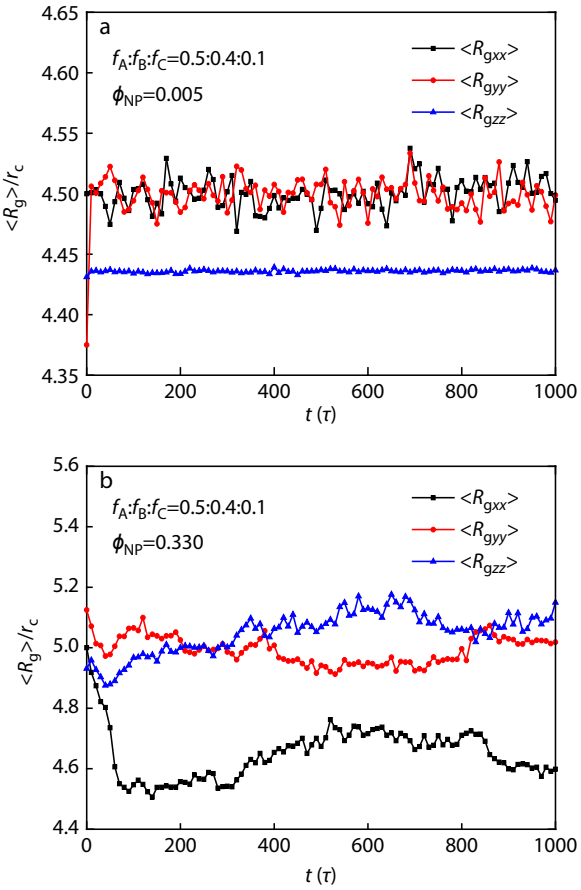

Fig. 7 The average radius of gyration $\mathbf{R}_g^2$ of LAM with the volume fractions of f_A:f_B:f_C=0.5:0.4:0.1 Three components are shown for the radius of gyrations at two cases in the dynamics processes, (a) the low NP concentration of Φ_{NP} = 0.005 and (b) the high NP concentration of Φ_{NP} = 0.330.

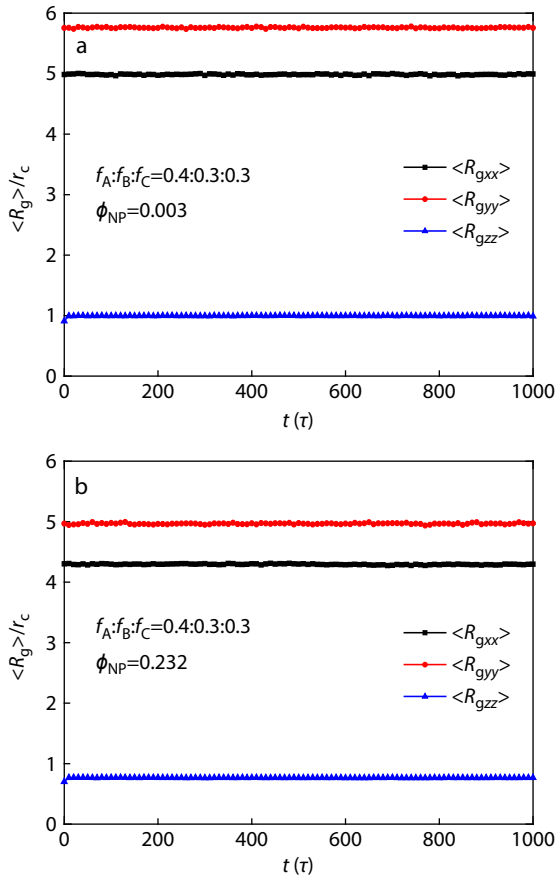

Fig. 8 The average radius of gyration $\mathbf{R}_g^2$ of PT with the volume fractions of f_A:f_B:f_C=0.4:0.3:0.3 Three components are shown for the radius of gyrations at two cases in the dynamics processes, (a) the low NP concentration of Φ_{NP} = 0.003 and (b) the high NP concentration of Φ_{NP} = 0.232.

of NPs is small, the average value of R_{gxx} and R_{gyy} is relatively close, but R_{gxx} less than R_{gyy}, R_{gxx} and R_{gyy} far greater than R_{gzz}. It indicates that the PT structure is relatively stretched in the *x*-and *y*-directions, but relatively tight along the *z*-direction. In fact, ABC star triblock copolymer self-assembly into PT structure, that is, the situation without NPs and low-concentration NPs are similar, and the average value of R_{gxx} and R_{gyy} is relatively close, but R_{gxx} less than R_{gyy}, R_{gxx} and R_{gyy} is also much larger than R_{gzz}, and they are also close numerically. This phenomenon indicates that the addition of a small number of NPs has no significant effect on the structure of PT. When the volume fraction of NPs reaches Φ_{NP} = 0.232, as shown in Fig. 8(b), high-concentration NPs do not have a large impact on the structure of PT, and the trend is consistent. The average value of R_{gxx} and R_{gyy} is relatively close, but R_{gxx} less than R_{gyy}, R_{gxx} and R_{gyy} far greater than R_{gzz}. It indicates that the PT structure is still relatively stretched in the *x*-direction and *y*-direction, and relatively tight along the *z*-direction. However, the values of the three components are all lower than those of the filled low-concentration NPs. These phenomena indicate that the addition of a large number of NPs has no obvious influence on the structure of PT, but the aggregation of NPs compresses the structure of PT more closely.

To further describe the changes in the shape of ABC star triblock copolymer, we extracted the shape factor of the polymer molecules from the average radius of gyrations. Shape factor $\langle\delta\rangle$ can be expressed as follows:[86,87]

$$\langle\delta\rangle = 1 - 3\left\langle\frac{L_1^2L_2^2 + L_1^2L_3^2 + L_2^2L_3^2}{\left(L_1^2+L_2^2+L_3^2\right)}\right\rangle \quad (13)$$

where L_1^2, L_2^2, and L_3^2 are the three eigenvalues of the gyration radius tensor $\mathbf{R}_g^2$. For the special conformation, we noted that the polymer chain had a spherical shape at $\langle\delta\rangle$ = 0 and the polymer chain had a circular shape at $\langle\delta\rangle$ = 0.5. Meanwhile, the polymer chain had a rod-like shape at $\langle\delta\rangle$ = 1, and the polymer chain formed ellipses when $\langle\delta\rangle$ was between 0 and 1.[88]

We plotted the variation of the shape factors in the self-assembly process of lamellar structure and NPs at different concentrations. As shown in Fig. 9, in the absence of NPs, the initial value of shape factor was $\langle\delta\rangle$ = 0.450, and $\langle\delta\rangle$ = 0.445 when the system was in equilibrium, indicating that the ABC star triblock copolymer chain always had an elliptical conformation. This result was similar to previous simulation observations.[79] For low-concentration NPs, $\langle\delta\rangle$ fluctuated around 0.375, indicating that the conformation of ABC star

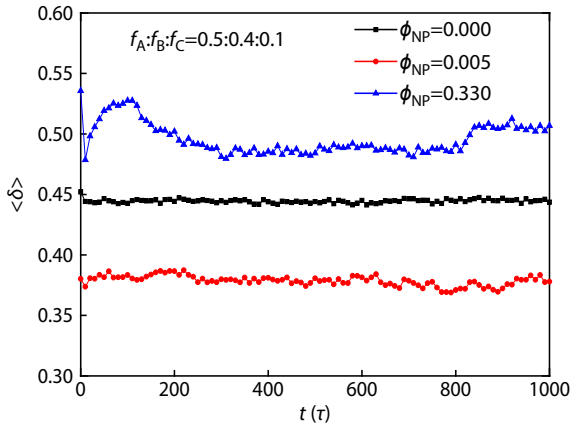

Fig. 9 The shape factor <δ> as function of time steps for LAM with the volume fractions of f_A:f_B:f_C=0.5:0.4:0.1, at the NP concentration of Φ_{NP} = 0.000, 0.005, 0.330, respectively.

triblock copolymer chain was also elliptical, but the chain was relatively compact. However, the addition of high-concentration NPs made the ABC star triblock copolymer undergo special changes. In particular, the shape factor was $\langle\delta\rangle$ = 0.540 in the beginning; $\langle\delta\rangle$ first decreased in the initial stage of t = 0−230τ, subsequently increased, and finally decreased again, indicating that the ABC star triblock copolymer chain continued to evolve. At t = 230−830τ, $\langle\delta\rangle$ was about 0.490; the ABC star triblock copolymer chains tended to have a circular conformation, and the system was stable at t = 830−1000τ, where $\langle\delta\rangle$ increased to 0.510. In this stage, the ABC star triblock copolymer chain also had an approximately circular conformation, but it was more relaxed than the mutual adaptation stage. This result was similar to the dynamic process observed in phospholipids under shear.[89] Polymer chains all have an elliptical conformation during evolution, and in our study, the chain conformation changes more gently.

Mechanical Properties of ABC Star Triblock Copolymers

In this subsection, we took the LAM structure as an example to investigate the mechanical properties under the influence of different NP concentrations and stiffness. We investigated the mechanical properties by the interfacial tension.[40,73,90,91] Based on the Irving-Kirkwood theory, we can define the tension formula σ_x along the x-direction:[92–94]

$$\sigma_x = \langle p_{xx}\rangle - \frac{1}{2}\left(\langle p_{yy}\rangle + \langle p_{zz}\rangle\right) \tag{14}$$

where the component of the pressure tensor p_{xx} can be achieved as follows:

$$p_{xx} = \frac{1}{V}\left\langle \sum_{i=1}^{N_p} m_i v_{ix} v_{ix} + \sum_{i=1}^{N_p}\sum_{j>1}^{N_p} F_{ijx} x_{ij} \right\rangle \tag{15}$$

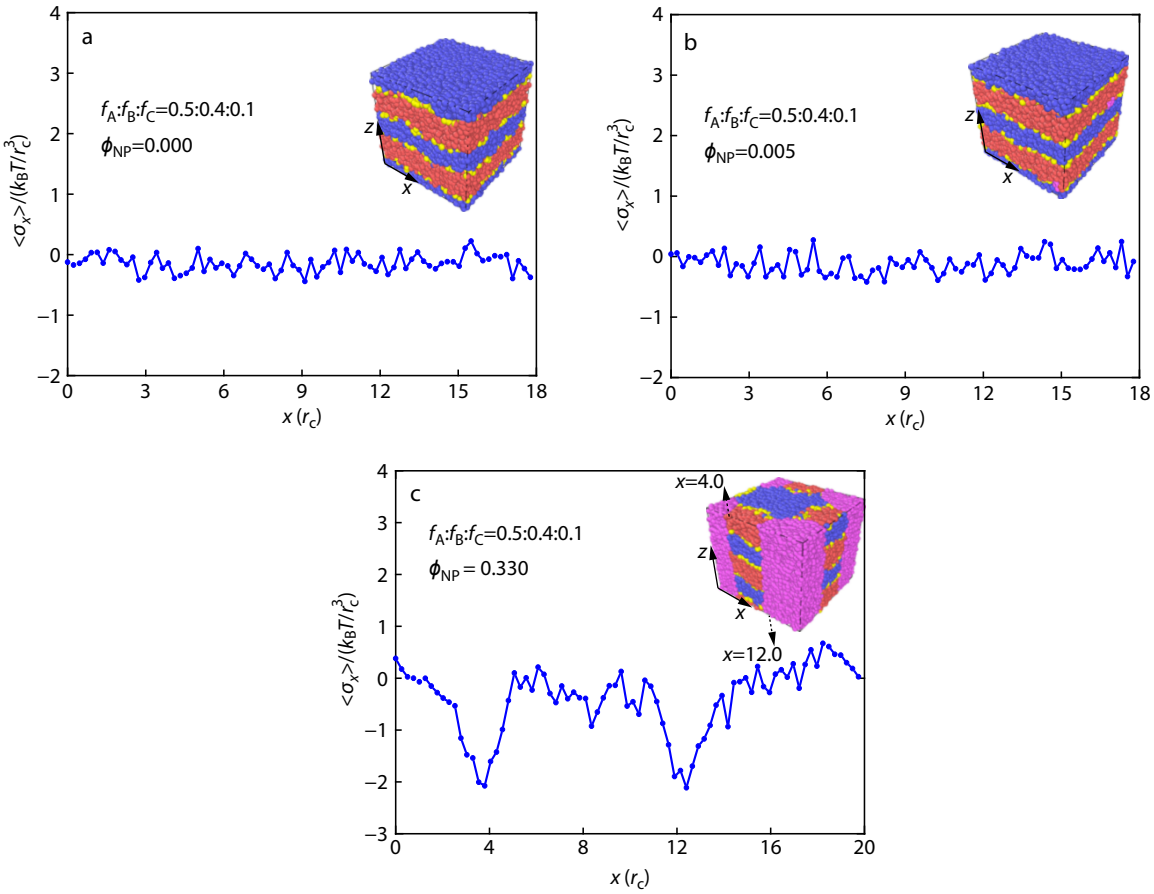

Fig. 10 The interface tension <σ_x> as function of distance along x-direction for LAM with the volume fractions of f_A:f_B:f_C=0.5:0.4:0.1, at (a–c) the volume fractions of NPs Φ_{NP}=0.000, 0.005, 0.330, respectively. The typical morphologies are also inserted.

https://doi.org/10.1007/s10118-023-3021-4

where V is the system volume, N_p is the number of DPD beads, and x_{ij} is the displacement between the i^{th} and j^{th} beads in the x-direction. F_{ijx} is the force between the i^{th} and j^{th} beads in the x-direction. The elements p_{yy} and p_{zz} are similar to p_{xx}, which have similar expressions in Eq. (14), only replaced by the corresponding subscripts.

The mechanical properties for the lamellar structures are shown in Fig. 10, with the volume fractions f_A:f_B:f_C=0.5:0.4:0.1 and Φ_{NP}=0.000, 0.005, 0.330, respectively. Fig. 10(b) shows the addition of NPs (Φ_{NP} = 0.005), where the value of σ_x oscillated around 0, indicating that the interfacial tension of the lamellar structure was about 0, so that it was basically in a no-pressure state. Indeed, as shown in Fig. 10(a), the lamellar structure had no interfacial tension without adding the NPs (Φ_{NP} = 0.000), which has been observed in some membranes.[74,75,95] Herein, our observations indicated that the small numbers of NPs were unable to influence the interfacial tensions. However, when in the number of NPs was increased to a large value, for example, when Φ_{NP} = 0.330, the co-assembly led to variations in the structures of triblock copolymers and resulted in changes in interfacial tension, as shown in Fig. 10(c). It can be observed that the value of σ_x appeared only as the minimum value near $x = 4.0r_c$ and $x = 12.0r_c$, and other positions oscillated around zero. These results showed that the surface tension was not zero at the interfaces between the different lamellar domains, but no interfacial tension existed within the cylinder where NPs were gathered and the lamellar domains were located. While $x = 4.0r_c$ and $x = 12.0r_c$ are at the junction of the columnar structure formed by NPs and the lamellar structure, therefore, σ_x will have a sudden change. Previous SCFT calculation and MC simulation studies also report zero interfacial tensions at the interfaces between two different domains in NP-filled diblock copolymers, thereby confirming our DPD results.[96,97]

Additionally, we investigated the interfacial tensions in the LAM structures with different chain flexibilities for ABC star triblock copolymers, and results are shown in Fig. 11. We took κ = 0.5 as the flexibility chain and κ = 10.0 as the rigidity one. For the first case shown in Fig. 11(a), we set the A-block to be κ = 0.5 and 10.0, whereas the B- and C-blocks were completely flexible. When only the A-blocks varied their chain form from flexible to rigid, the interfacial tension σ_z changed near the boundaries of the A- and B-block domains. We observed similar variations in the interfacial tension σ_z when the stiffnesses were κ=0.5 and 10.0, as shown in Fig. 11(a). This behavior also appeared in the diblock copolymers where the chains were flexible.[96,97] To examine the star topology in the triblock copolymers, we changed the chain flexibilities for B- and C-blocks, as shown in Fig. 11(b). We observed that the variations were not obvious for the rigidity case than those in

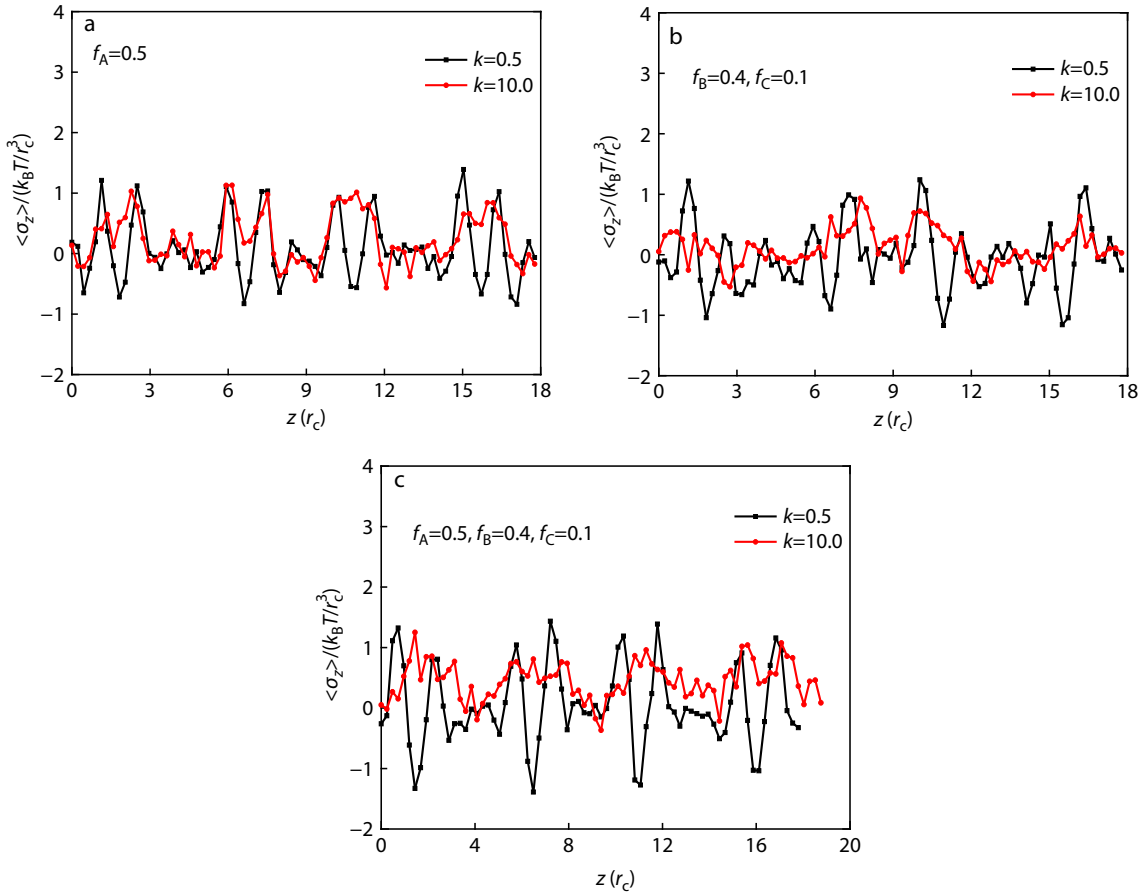

Fig. 11 The interface tension $<\sigma_z>$ as function of time steps for LAM with the volume fractions of f_A:f_B:f_C=0.5:0.4:0.1, at two different stiffness κ = 0.5, 10.0. (a) The stiffness of A-block, (b) the stiffness of B- and C-block, and (c) the stiffness of A-, B- and C-block.

https://doi.org/10.1007/s10118-023-3021-4

the flexibility case. In other words, the ABC star triblock copolymers exhibited obvious interfacial tensions between the different block domains when the chains were flexible. When we changed the flexibilities for all A-, B- and C-blocks, the variations in interfacial tension σ_z became more obvious, as shown in Fig. 11(c). In particular, the interfacial tension σ_z changed smoothly across the interfaces between two domains when $\kappa=10.0$ but more drastically when $\kappa=0.5$. In the flexibility case, the chains stretched more completely and had greater interfacial width than those in the rigidity case, leading to obvious variations between the two domains in the flexibility case.

CONCLUSIONS

We investigated the co-assembly of NP-filled ABC star triblock copolymers through CG model-based DPD simulation. We selected the LAM and PT structures to examine the filling effects of NPs in two cases, the low- and high-concentration NPs. We investigated the co-assembly for the ABC star triblock copolymers and NPs in equilibrium states and dynamic processes. We also evaluated the mechanical properties of ABC star triblock copolymers by using interfacial tensions.

For the equilibrium states, a low NP concentration was unable to affect the LAM and PT structures of ABC star triblock copolymers, whereas the LAM and PT directed the NPs to distribute between the interfaces among the different domains. However, the high NP concentrations affected the LAM and PT structures in different ways. In LAM structures, the NPs were forced into four cylindrical zones and coexisted with the polymer LAM, whereas the NPs were still distributed at the interfaces between the tiling domains at high NP concentrations. Such different aggregation behaviors were due to the strong star-topology confinement in the tiling structures of the triblock copolymers. The repulsive interactions between the different beads of DPD tend to separate the different blocks, and the star topology, which is the presence of the heart knot in the copolymer, gives the copolymer connectivity and prevents its macroscopic separation. We subsequently investigated the dynamic processes of the NP-filled LAM and PT structures for ABC star triblock copolymers. The dynamic processes can be sorted into three stages, *i.e.*, the initial, adjustment, and stable stages, in low and high NP concentrations. For LAM structures, the energy of the system is lower and the time to reach equilibrium is shorter when the low-concentration NPs are added. According to the radius of rotation and shape factor, the addition of a small number of NPs has no significant effect on the microstructure. When high-concentration NPs are added, the energy of the system is higher, the structure is destroyed, and the time to reach equilibrium becomes longer. The observation of gyration radius shows that the high-concentration NPs have a strong effect on the molecular conformation of ABC star triblock copolymer, which is further confirmed by the results of shape factor. For PT structures, the filled of low-concentration NPs is similar to that of high-concentration NPs. The radius of rotation indicate that the PT structure is only compressed more tightly when filled with a large number of NPs. The dynamic process and chain conformation of the two microstructures are compared, and it is found that the PT structure is more stable than the LAM structure. Moreover, we investigated the mechanical properties by analyzing the interfacial tensions for the LAM structures. Results showed that the surface tension was not zero at interfaces between the different lamellar domains, but no interfacial tension existed within the cylinder where NPs were gathered and the lamellar domains were located. In particular, the interfacial tension σ_z changed smoothly across the interfaces between two domains at the rigidity of $\kappa=10.0$ but more drastically at the flexible case with $\kappa=0.5$, in which the chains were stretched more completely and had greater interfacial width than those in the rigidity case, leading to obvious variations between the two domains. It should be pointed out that although the simple NP modelling can describe the main features of NPs in the current simulations, this model cannot characterize the effects of the size and shape of NPs. We still need to model the complex NP in the future. For example, if the NPs can reach block size, it can be predicted that the NPs may cause more severe deformation of the structure and hinder the self-assembly of the star triblock copolymer, which is a topic worthy of further investigation. We expect abundant microstructures with various NP concentrations to predict the dynamic processes and mechanical properties in the future and thus provide a deeper understanding of the co-assembly of block copolymers with special topologies.

Conflict of Interests

The authors declare no interest conflict.

ACKNOWLEDGMENTS

This work was financially supported by the National Natural Science Foundation of China (No. 11875205).

REFERENCES

1 Guo, Z. J.; Zhang, G. J.; Qiu, F.; Zhang, H. D.; Yang, Y. L. Discovering ordered phases of block copolymers: new results from a generic Fourier-space approach. *Phys. Rev. Lett.* **2008**, *101*, 028301.
2 Bates, F. S.; Hillmyer, M. A.; Lodge, T. P.; Bates, C. M.; Delaney, K. T.; Fredrickson, G. H. Multiblock polymers: Panacea or Pandora's box. *Science* **2012**, *336*, 434.
3 Yabu, H.; Higuchi, T.; Jinnai, H. Frustrated phases: polymeric self-assemblies in a 3D confinement. *Soft Matter* **2014**, *10*, 2919–2931.
4 Zhang, Q.; Lin, J. P.; Wang, L. Q.; Xu, Z. W. Theoretical modeling and simulations of self-assembly of copolymers in solution. *Prog. Polym. Sci.* **2017**, *75*, 1–30.
5 Conka, R.; Marien, Y. W.; Sedlacek, O; Hoogenboom, R.; Van Steenberge, P. H. M.; D'Hooge, D. R. A unified kinetic Monte Carlo approach to evaluate (a)symmetric block and gradient copolymers with linear and branched chains illustrated for poly(2-oxazoline)s. *Polym. Chem.* **2022**, *13*, 1559–1575.
6 Matsushita, Y. Creation of hierarchically ordered nanophase structures in block polymers having various competing interactions. *Macromolecules* **2007**, *40*, 771–776.
7 Takano, A.; Wada, S.; Sato, S.; Arak, T.; Hirahara, K.; Kazama, T.; Kawahara, S.; Isono, Y.; Ohno A.; Tanaka, N.; Matsushita, Y. Observation of cylinder-based microphase-separated structures from ABC star-shaped terpolymers investigated by electron

computerized tomography. *Macromolecules* **2004**, *37*, 9941–9946.
8 Hayashida, K.; Kawashima, W.; Takano, A.; Shinohara, Y.; Amemiya, Y.; Nozue, Y.; Matsushita, Y. Archimedean tiling patterns of ABC star-shaped terpolymers studied by microbeam small-angle X-ray scattering. *Macromolecules* **2006**, *39*, 4869–4872.
9 Hayashida, K.; Takano, A.; Arai, S.; Shinohara, Y.; Amemiya, Y.; Matsushita, Y. Systematic transitions of tiling patterns formed by ABC star-shaped terpolymers. *Macromolecules* **2006**, *39*, 9402–9408.
10 Tang, P.; Qiu, F.; Zhang, H. D.; Yang, Y. L. Morphology and phase diagram of complex block copolymers: ABC star triblock copolymers. *J. Phys. Chem. B* **2004**, *108*, 8434–8438.
11 Zhang, G. J.; Qiu, F.; Zhang, H. D.; Yang, Y. L.; Shi, A. C. SCFT study of tiling patterns in ABC star terpolymers. *Macromolecules* **2010**, *43*, 2981–2989.
12 Li, S. B.; Qiu, W. J.; Zhang, L. X.; Liang, H. J. Nanostructures and phase diagrams of ABC star triblock copolymers in pore geometries. *J. Chem. Phys.* **2012**, *136*, 124906.
13 Jiang, K.; Zhang, J.; Liang, Q. Self-assembly of asymmetrically interacting ABC star triblock copolymer melts. *J. Phys. Chem. B* **2015**, *119*, 14551–14562.
14 Huang, C. I.; Fang, H. K.; Lin, C. H. Morphological transition behavior of ABC star copolymers by varying the interaction parameters. *Phys. Rev. E* **2008**, *77*, 031804.
15 Moniruzzaman, M.; Winey, K. I. Polymer nanocomposites containing carbon nanotubes. *Macromolecules* **2006**, *39*, 5194–5205.
16 Schacher, F. H.; Rupar, P. A.; Manners, I. Functional block copolymers: nanostructured materials with emerging applications. *Angew. Chem. Int. Ed.* **2012**, *51*, 7898–7921.
17 Kao, J.; Thorkelsson, K.; Bai, P.; Rancatore, B. J.; Xu, T. Toward functional nanocomposites: taking the best of nanoparticles, polymers, and small molecules. *Chem. Soc. Rev.* **2013**, *42*, 2654–2678.
18 Kumar, S. K.; Jouault, N.; Benicewicz, B.; Neely, T. Nanocomposites with polymer grafted nanoparticles. *Macromolecules* **2013**, *46*, 3199–3214.
19 Hagita, K.; Morita, H.; Takano, H. Molecular dynamics simulation study of a fracture of filler-filled polymer nanocomposites. *Polymer* **2016**, *99*, 368–375.
20 Chai, S. C.; Cao, X.; Xu, F. R.; Zhai, L.; Qian, H. J.; Chen, Q.; Wu, L. X.; Li, H. L. Multiscale self-assembly of mobile-ligand molecular nanoparticles for hierarchical nanocomposites. *ACS Nano* **2019**, *13*, 7135–7145.
21 Liu, M. H.; Li, S.; Fang, Y.; Chen, Z. D.; Alyas, M.; Liu, J.; Zeng, X. F.; Zhang, L. Q. Mechanical and self-healing behavior of matrix-free polymer nanocomposites constructed *via* grafted graphene nanosheets. *Langmuir* **2020**, *36*, 7427–7438.
22 Zhao, D.; Di Nicola, M.; Khani, M. M.; Jestin, J.; Benicewicz, B. C.; Kumar, S. K. Role of block copolymer adsorption versus bimodal grafting on nanoparticle self-assembly in polymer nanocomposites. *Soft Matter* **2016**, *12*, 7241–7247.
23 Chiu, J. J.; Kim, B. J.; Kramer, E. J.; Pine, D. J. Control of nanoparticle location in block copolymers. *J. Am. Chem. Soc.* **2005**, *127*, 5036–5037.
24 Chen, S.; Guo, C.; Hu, G.-H.; Liu, H. Z.; Liang, X. F.; Wang, J.; Ma, J. H. Zheng, L. Dissipative particle dynamics simulation of gold nanoparticles stabilization by PEO-PPO-PEO block copolymer micelles. *Colloid Polym. Sci.* **2007**, *285*, 1543–1552.
25 Deshmukh, R. D.; Buxton, G. A.; Clarke, N.; Composto, R. J. Nanoscale block copolymer templates decorated by nanoparticle arrays. *Macromolecules* **2007**, *40*, 6316–6324.
26 Chen, H.Y.; Ruckenstein, E. Nanoparticle aggregation in the presence of a block copolymer. *J. Chem. Phys.* **2009**, *131*, 244904.
27 Chen, H. Y.; Ruckenstein, E. Structure and particle aggregation in block copolymer-binary nanoparticle composites. *Polymer* **2010**, *51*, 5869–5882.
28 Lo, C. T.; Lee, B.; Pol, V. G.; Dietz Rago, N. L.; Seifert, S.; Winans, R. E.; Thiyagarajan, P. Effect of molecular properties of block copolymers and nanoparticles on the morphology of self-assembled bulk nanocomposites. *Macromolecules* **2007**, *40*, 8302–8310.
29 Xiang, W. J.; Zhu, Z. J.; Song, X. Y.; Zhong, C.; Wang, C. J.; Ma, Y. Z. Concentration-induced structural transition of block polymer self-assemblies on a nanoparticle surface: computer simulation. *RSC Adv.* **2016**, *6*, 102057–102067.
30 Krook, N. M.; Ford, J.; Marechal, M.; Rannou, P.; Meth, J. S.; Murray, C. B.; Composto, R. J. Alignment of nanoplates in lamellar diblock copolymer domains and the effect of particle volume fraction on phase behavior. *ACS Macro Lett.* **2018**, *7*, 1400–1407.
31 Martín-García, B.; Velázquez, M. M. Block copolymer assisted self-assembly of nanoparticles into Langmuir-Blodgett films: effect of polymer concentration. *Mater. Chem. Phys.* **2013**, *141*, 324–332.
32 Coleman, B. R.; Moffitt, M. G. Amphiphilic inorganic nanoparticles with mixed polymer brush layers of variable composition: bridging the paradigms of block copolymer and nanoparticle self-assembly. *Chem. Mater.* **2018**, *30*, 2474–2482.
33 Huang, J. H.; Fan, Z. X.; Luo, M. B. Simulation study on the structure of rod-coil-rod triblock copolymer and nanoparticle mixture within slit. *J. Chem. Phys.* **2013**, *139*, 204904.
34 Zhao, D.; Di Nicola, M.; Khani, M. M.; Jestin, J.; Benicewicz, B.C.; Kumar, S. K. Self-assembly of monodisperse versus bidisperse polymer-grafted nanoparticles. *ACS Macro Lett.* **2016**, *5*, 790–795.
35 Shi, R.; Qian, H. J.; Lu, Z. Y. Computer simulation study on the self-assembly of unimodal and bimodal polymer-grafted nanoparticles in a polymer melt. *Phys. Chem. Chem. Phys.* **2017**, *19*, 16524–16532.
36 Tripathy, M. Self-assembly of polymer-linked nanoparticles and scaling behavior in the assembled phase. *Soft Matter* **2017**, *13*, 2475–2482.
37 Xu, P. X.; Lin, J. P.; Zhang, L. S. Distinct viscoelasticity of nanoparticle-tethering polymers revealed by nonequilibrium molecular dynamics simulations. *J. Phys. Chem. C* **2017**, *121*, 28194–28203.
38 Diaz, J.; Pinna, M.; Zvelindovsky, A.; Pagonabarraga, I. Co-assembly of Janus nanoparticles in block copolymer systems. *Soft Matter* **2019**, *15*, 6400–6410.
39 Yi, C. L.; Yang, Y. Q.; Liu, B.; He, J.; Nie, Z. H. Polymer-guided assembly of inorganic nanoparticles. *Chem. Soc. Rev.* **2020**, *49*, 465–508.
40 Liu, M.B.; Liu, G. R.; Zhou, L. W.; Chang, J. Z. Dissipative particle dynamics (DPD): an overview and recent developments. *Arch. Computat. Methods Eng.* **2015**, *22*, 529–556.
41 Espanol, P.; Warren, P. B. Perspective: dissipative particle dynamics. *J. Chem. Phys.* **2017**, *146*, 150901.
42 Ye, T.; Li, Y. A comparative review of smoothed particle hydrodynamics, dissipative particle dynamics and smoothed dissipative particle dynamics. *Int. J. Comput. Method* **2018**, *15*, 1850083.
43 Santo, K. P.; Neimark, A. V. Dissipative particle dynamics simulations in colloid and Interface science: a review. *Adv. Colloid Interface Sci.* **2021**, *298*, 102545.
44 Wang, J. H.; Han, Y. F.; Xu, Z. Y.; Yang, X. Z.; Ramakrishna, S.; Liu, Y. Dissipative particle dynamics simulation: a review on investigating mesoscale properties of polymer systems. *Macromol. Mater. Eng.* **2021**, *306*, 2000724.
45 Procházka, K.; Limpouchová, Z.; Štěpánek, M.; Šindelka, K.; Lísal, M. DPD modelling of the self- and co-assembly of polymers and

https://doi.org/10.1007/s10118-023-3021-4

polyelectrolytes in aqueous media: impact on polymer science. *Polymers* **2022**, *14*, 404.
46 Hoogerbrugge, P. J.; Koelman, J. M. V. A. Simulating microscopic hydrodynamic phenomena with dissipative particle dynamics. *Europhys. Lett.* **1992**, *19*, 155–160.
47 Groot, R.D.; Warren, P.B. Dissipative particle dynamics: Bridging the gap between atomistic and mesoscopic simulation. *J. Chem. Phys.* **1997**, *107*, 4423–4435.
48 Liu, H. J.; Cavaliere, S.; Jones, D. J.; Rozière, J.; Paddison, S. J. Scaling behavior of nafion with different model parameterizations in dissipative particle dynamics simulations. *Macromol. Theory Simul.* **2018**, *27*, 1800003.
49 Ortiz, V.; Nielsen, S. O.; Discher, D. E.; Klein, M. L.; Lipowsky, R.; Shillcock, J. Dissipative particle dynamics simulations of polymersomes. *J. Phys. Chem. B* **2005**, *109*, 17708–17714.
50 Schiller, U.D.; Krüger, T.; Henrich, O. Mesoscopic modelling and simulation of soft matter. *Soft Matter* **2018**, *14*, 9–26.
51 Zhang, L. Y.; Becton, M.; Wang, X. Q. Designing nanoparticle translocation through cell membranes by varying amphiphilic polymer coatings. *J. Phys. Chem. B* **2015**, *119*, 3786–3794.
52 Chaudhri, A.; Lukes, J. R. Velocity and stress autocorrelation decay in isothermal dissipative particle dynamics. *Phys. Rev. E* **2010**, *81*, 026707.
53 Plimpton, S. Fast parallel algorithms for short-range molecular dynamics. *J. Comput. Phys.* **1995**, *117*, 1–19.
54 Kong, W. X.; Li, B. H.; Jin, Q. H.; Ding, D. T; Shi, A. C. Helical vesicles, segmented semivesicles, and noncircular bilayer sheets from solution-state self-assembly of ABC miktoarm star terpolymers. *J. Am. Chem. Soc.* **2009**, *131*, 8503–8512.
55 Li, W. H.; Xu, Y. C.; Zhang, G. J.; Qiu, F.; Yang, Y. L.; Shi, A. C. Real-space self-consistent mean-field theory study of ABC star triblock copolymers. *J. Chem. Phys.* **2010**, *133*, 064904.
56 Li, S. B.; Jiang, Y.; Chen, J. Z.Y. Morphologies and phase diagrams of ABC star triblock copolymers confined in a spherical cavity. *Soft Matter* **2013**, *9*, 4843–4854.
57 Pogodin, S.; Bauli, V. A. Equilibrium insertion of nanoscale objects into phospholipid bilayers. *Curr. Nanosci.* **2011**, *7*, 721.
58 Sun, L. L.; Pan, F.; Li, S. B. Self-assembly of lipid mixtures in solutions: structures, dynamics processes and mechanical properties. *Membranes* **2022**, *12*, 730.
59 Chremos, A.; Theodorakis, P. E. Impact of intrinsic backbone chain stiffness on the morphologies of bottle-brush diblock copolymers. *Polymer* **2016**, *97*, 191–195.
60 Singh, A.; Chakraborti, A.; Singh, A. Role of a polymeric component in the phase separation of ternary fluid mixtures: a dissipative particle dynamics study. *Soft Matter* **2018**, *14*, 4317–4326.
61 Lin, S. L.; Xu, M. Y.; Yang, Z. R. Dissipative particle dynamics study on the mesostructures of *n*-octadecane/water emulsion with alternating styrene–maleic acidcopolymers as emulsifier. *Soft Matter* **2012**, *8*, 375–384.
62 Ding, H. M.; Ma, Y. Q. Theoretical and computational investigations of nanoparticle-biomembrane interactions in cellular delivery. *Small* **2015**, *11*, 1055–1071.
63 Xia, P. P.; Shan, Y.; He, L. L.; Ji, Y. Y.; Wang, X. H.; Li, S. B. Multinanoparticle translocations in phospholipid membranes: translocation modes and dynamic processes. *Chin. J. Chem. Phys.* **2020**, *33*, 468–476.
64 Kravchenko, V. S.; Potemkin, I. I. Self-assembly of rarely polymer-grafted nanoparticles in dilute solutions and on a surface: from non-spherical vesicles to graphene-like sheets. *Polymer* **2018**, *142*, 23–32.
65 Cho, H. K.; Ch, I. W.; Lee, J. M.; Kim, J. H. Polymeric nanoparticles, micelles and polymersomes from amphiphilic block copolymer. *Korean J. Chem. Eng.* **2010**, *27*, 731–740.
66 Chen, H.; Ruckenstein, E. Aggregation of nanoparticles in a block copolymer bilayer. *J. Colloid Interface Sci.* **2011**, *363*, 573–578.
67 Yang, J. Y.; Hu, Y.; Wang, R.; Xie, D. Q. Nanoparticle encapsulation in vesicles formed by amphiphilic diblock copolymers. *Soft Matter* **2017**, *13*, 7840–7847.
68 Abu-Nada, E.; Pop, I.; Mahian, O. A dissipative particle dynamics two-component nanofluid heat transfer model: application to natural convection. *Int. J. Heat and Mass Transfer* **2019**, *133*, 1086–1098.
69 Jia, L.; Wang, R.; Fan, Y. N. Encapsulation and release of drug nanoparticles in functional polymeric vesicles. *Soft Matter* **2020**, *16*, 3088–3095.
70 Nam, C.; Lee, W. B.; Kim, Y. Self-assembly of rod-coil diblock copolymer-nanoparticle composites in thin films: dissipative particle dynamics. *Soft Matter* **2021**, *17*, 2384–2391.
71 Li, Z.; Wang, J. F.; Wei, Q.; Qi, Z. Q.; Zhou, L. X.; Li, J. W. In silico insights into the receptor-mediated endocytosis of virus-like nanoparticles. *Chem. Phys. Lett.* **2022**, *790*, 139360.
72 Song, W. Y.; Lu, H.; He, J. W.; Zhu, Z. J.; He, S. Y.; Liu, D. H.; Liu, H.; Wang, Y. Dynamics and morphology of self-assembly behavior of polymer-grafted nanoparticles: a dissipative particle dynamics simulation study. *Polym. Int.* **2022**, *71*, 1330–1339.
73 Maiti, A.; McGrother, S. Bead-bead interaction parameters in dissipative particle dynamics: relation to bead-size, solubility parameter, and surface tension. *J. Chem. Phys.* **2004**, *120*, 1594–1601.
74 Qiang, X. W.; Wang, X. H.; Ji, Y. Y.; Li, S. B.; He, L. L. Liquid-crystal self-assembly of lipid membranes on solutions: a dissipative particle dynamic simulation study. *Polymer* **2017**, *115*, 1–11.
75 Chen, Y. Y.; Wang, Z. G.; Ji, Y. Y.; He, L. L.; Wang, X. H.; Li, S. B. Asymmetric lipid membranes under shear flows: a dissipative particle dynamics study. *Membranes* **2021**, *11*, 655.
76 Velázquez, M. E.; Gama-Goicochea, A.; González-Melchor, M.; Neria, M.; Alejandre, J. Finite-size effects in dissipative particle dynamics simulations. *J. Chem. Phys.* **2006**, *124*, 084104.
77 Matsen, M. W.; Thompson, R. B. Particle distributions in a block copolymer nanocomposite. *Macromolecules* **2008**, *41*, 1853–1860.
78 Thompson, R. B.; Ginzburg, V. V.; Matsen, M. W.; Balazs, A. C. Predicting the mesophases of copolymer-nanoparticle composites. *Science* **2001**, *292*, 2469.
79 Kang, H.; Detcheverry, F. A.; Mangham, A. N.; Stoykovich, M. P.; Daoulas, K. C.; Hamers, R. J.; Müller, M.; de Pablo, J. J.; Nealey, P. F. Hierarchical assembly of nanoparticle superstructures from block copolymer-nanoparticle composites. *Phys. Rev. Lett.* **2008**, *100*, 148303.
80 Lo, C. T.; Lee, B.; Dietz Rago, N. L; Winans, R. E.; Thiyagarajan, P. Strategy for better ordering in diblock copolymer based nanocomposites. *Macromol. Rapid Commun.* **2007**, *28*, 1607–1612.
81 He, L. L.; Zhang, L. X.; Liang, H. J. The effects of nanoparticles on the lamellar phase separation of diblock copolymers. *J. Phys. Chem. B* **2008**, *112*, 4194–4203.
82 Tang, Q. Y.; Ma, Y. Q. Self-assembly of rod-shaped particles in diblock-copolymer templates. *J. Phys. Chem. B* **2009**, *113*, 10117–10120.
83 Huang, W.; Zaburdaev, V. The shape of pinned forced polymer loops. *Soft Matter* **2019**, *15*, 1785–1792.
84 Haller, G. Dynamic rotation and stretch tensors from a dynamic polar decomposition. *J. Mech. Phys. Solids* **2016**, *86*, 70–93.
85 Shan, Y.; Ji, Y. Y.; Wang, X. H.; He, L. L.; Li, S. B. Predicting asymmetric phospholipid microstructures in solutions. *RSC Adv.* **2020**, *10*, 24521–24532.
86 Zifferer, G.; Preusser, W. Monte Carlo simulation studies of the size and shape of ring polymers. *Macromol. Theory Simul.* **2001**,

10, 397–407.
87 Diehi, H.W.; Eisenriegler, E. Universal shape ratios for open and closed random walks: exact results for all d. *J. Phys. A* **1989**, *22*, L87–L91.
88 Li, S. B.; Zhang, L. X. Conformational structures and thermodynamic properties of compact polymer chains confined between two parallel plane boundaries. *J. Polym. Sci. B* **2006**, *44*, 2888–2901.
89 Shan, Y.; Qiang, X. W.; Ye, J. Z.; Wang, X. H.; He, L. L.; Li, S. B. Shear-induced microstructures and dynamics processes of phospholipid cylinders in solutions. *Sci. Rep.* **2019**, *9*, 15393.
90 Villers, D.; Flatten, J. K. Temperature dependence of the interfacial tension between water and long-chain alcohols. *J. Phys. Chem.* **1988**, *92*, 4023–4024.
91 Petelska, A. D. Interfacial tension of bilayer lipid membranes. *Cent. Eur. J. Chem.* **2012**, *10*, 16–26.
92 Irving, J. H.; Kirkwood, J. G. The Statistical mechanical theory of transport processes. IV. The equations of hydrodynamics. *J. Chem. Phys.* **1950**, *18*, 817–829.
93 Yang, J. Z. J; Wu, X. J.; Li, X. T. A generalized Irving-Kirkwood formula for the calculation of stress in molecular dynamics models. *J. Chem. Phys.* **2012**, *137*, 134104.
94 Smith, E. R.; Heyes, D. M.; Dini, D. Towards the Irving-Kirkwood limit of the mechanical stress tensor. *J. Chem. Phys.* **2017**, *146*, 224109.
95 Yamamoto, T.; Safran, S. A. Line tension between domains in multicomponent membranes is sensitive to degree of unsaturation of hybrid lipids. *Soft Matter* **2011**, *7*, 7021–7033.
96 Maniadis, P.; Lookman, T.; Kober, E. M.; Rasmussen, K. Ø. Stress distributions in diblock copolymers. *Phys. Rev. Lett.* **2007**, *99*, 048302.
97 Detcheverry, F. A.; Pike, D. Q.; Nealey, P. F.; Müller, M.; de Pablo, J. J. Monte Carlo simulation of coarse grain polymeric systems. *Phys. Rev. Lett.* **2009**, *102*, 197801.

https://doi.org/10.1007/s10118-023-3021-4